MSDE

PAPER

View Article Online
View Journal | View Issue



Cite this: *Mol. Syst. Des. Eng.*, 2021, **6**, 381

# Donor-free oligothiophene based dyes with di-anchor architecture for dye-sensitized solar cells†

John Marques dos Santos,‡[a] Ellie Tanaka, ‡[b] Alan A. Wiles,[a] Graeme Cooke *[a] and Neil Robertson *[b]

Received 16th February 2021,
Accepted 17th March 2021

DOI: 10.1039/d1me00009h

rsc.li/molecular-engineering

Traditionally, metal free DSSCs are fabricated from sensitizers designed using a donor–pi–acceptor (D–π–A) architecture. More recently, non-conventional dyes without strong donor units have emerged and have provided competitive power conversion efficiencies (PCEs) with respect to their (D–π–A)-based counterparts. Here, we report the synthesis and DSSC fabrication of oligothiophene molecules featuring two anchoring groups that do not possess strong donor moieties and are able to adopt V- and U-shape conformations. PCEs of 3.70% were obtained with the smaller 5-thiophene dyes (**5T2A**, **5T2A-E**) possessing higher PCEs than their larger 8-thiophene counterparts containing diacetylene units (**8T4A**, **8T4A-E**). Comparison to the DSSC properties of the analogous linear dye **5T**, indicates that the architecture and structure of this series of dyes are likely responsible for their lower performance.

### Design, System, Application

We have designed and synthesised two generations of oligothiophene dyes that do not possess strong donor units and incorporate two peripheral anchoring groups to investigate this type of functionalisation for inexpensive sensitisers for dye-sensitised solar cells (DSSCs). The molecules can adopt V- and U-shape conformations, which is desirable for a di-anchoring process, and benefit from slight bathochromic shifts upon ethylenedioxythiophene (EDOT) functionalisation. We find that the larger 8-thiophene dyes display slightly blue-shifted spectra compared with their 5-thiophene counterparts due to the presence of diacetylene residues, and poorer performances likely due to dye architecture as will be discussed in depth. This work provides valuable guidance towards improving the design and performance of inexpensive "donor-free" thiophene-based dyes for DSSCs.

## 1. Introduction

Dye-sensitized solar cells (DSSCs) continue to attract significant attention in endeavours to harness the considerable potential of solar radiation to provide renewable energy. It has been shown that the correct molecular engineering of sensitizers can greatly improve the performance of these solar energy conversion devices.[1,2] The overall power conversion efficiency (PCE, η) has been raised from about 7% to *circa* 14% since this technology emerged, and DSSCs have also proven to be a very promising technology for low light scenarios such as indoor applications.[3–5] Significant effort continues to be directed towards improving the PCE of DSSCs by modifying the electrolyte and sensitizers,[6–8] and structural modification of the latter continues to be an attractive way to increase this parameter.[6,9–11]

As the central component of DSSCs, the sensitizer harvests sunlight which leads to the production of photon-excited electrons. It is noteworthy that efficient electron injection from the excited dye to the conduction band of the $TiO_2$ through the anchoring group is achieved using dyes with a D–π–A (D = electron donor, A = electron acceptor/anchoring group) archictecture.[12] However, it has been shown in recent reports that outstanding efficiencies can be reached with dyes containing only thiophene π-bridges as relatively weak donors (referred to as "donor-free" dyes since they are absent of strong electron-donating moieties) with a general structure of $\pi_n$–A.[13,14] This indicated that these simple building blocks can be functionalised in simple ways to provide low-cost and efficient DSSCs. On the other hand, the choice of the anchoring group determines the electron injection rate in DSSCs devices.[15–18] It is also partially influential on the arrangement of the dyes in the monolayer anchored on the surface of the semiconductor.[19] Due to its strong electron-

[a] *School of Chemistry, Joseph Black Building, University of Glasgow, Glasgow, G12 8QQ, UK. E-mail: Graeme.Cooke@glasgow.ac.uk*
[b] *School of Chemistry, EaStCHEM, University of Edinburgh, King's Buildings, David Brewster Road, Edinburgh, Scotland EH9 3FJ, UK*

† Electronic supplementary information (ESI) available. See DOI: 10.1039/d1me00009h

‡ These authors contributed equally.

accepting character, strong binding interaction with the oxide and efficient electron injection, cyanoacetic acid is the most commonly used.[10,16,20–27]

In spite of these observations, single D–π–A dyes usually have a rod-shaped structure that facilitate dye loading; however, this may contribute to aggregation and charge recombination due to undesirable π–π stacking. Hence, considerable attention has been paid to dyes containing multiple anchoring groups,[26] since they show limited aggregation as well as increased electron extraction channels, enhanced binding strength, lower optical-gap and enhanced extinction coefficient thus enhancing the device performance.[2,28–31] In this regard, Eiamprasert *et al.* recently compared triphenylamine-based dyes with various anchoring groups and found the highest efficiency for the di-anchored dyes in comparison to the mono and the tri-anchored ones. The performance was also improved when an additional donor was incorporated into the semi-circular system.[32]

Here, to gain further insight into the design of 'donor-free' thiophene-based sensitizers, we present two generations of dyes featuring two anchoring cyanoacrylate acceptor units (Fig. 1). Despite the important advantages that the di-anchoring architecture can offer, it is so far not clear in the literature whether this structural feature would benefit "donor-free" thiophene-based dyes. Moreover, it is well-known that adjacent thiophenes preferably adopt an *anti*-conformation that usually leads oligothiophenes to adopt a linear conformation.[33,34] This suggests that to effectively di-anchor at the $TiO_2$ surface, these dyes would possibly have to overcome this rotational barrier.

The first-generation dyes were designed to be V-shaped if di-anchored (**5T2A** and **5T2A-E**) whereas the larger second-generation dyes (**8T4A** and **8T4A-E**), formed from precursors that were side products from the synthesis of the first-generation dyes, would adopt a more U-shaped conformation and feature diacetylene residues. Acetylenes in these molecules were designed to mitigate steric hindrance between moieties. These residues can compromise the intramolecular charge transfer (ICT) effect,[35] however they seem not to be detrimental for dye-sensitizers, since structures are sought after with permanent molecular dipole and several devices with high PCE include this architectural feature.[5,15,35–38] Furthermore, we have incorporated ethylenedioxythiophene (EDOT) residues into two of the dyes to increase the donor ability of one of the thiophenes units. We performed density functional theory (DFT) calculations to investigate the possibility of di-anchoring by accessing the number and distribution of possible molecular conformations, and investigated the DSSC properties of these sensitizers while comparing them to related linear donor-free dye **5T**.[13,14]

## 2. Results and discussion

### 2.1. Molecular design and synthesis

The first-generation of di-anchoring dyes (**5T2A**, **5T2A-E**) were designed to feature a conjugated system composed of 5 thiophene units, similar to dye **5T**. However, unlike **5T**, two acetylene residues were introduced to help to alleviate conformational strain and favour a di-anchoring conformation at the $TiO_2$ surface. To investigate the effect of additional thiophenes and additional acetylenes, the second-generation dyes (**8T4A** and **8T4A-E**) were designed to feature a conjugated system composed of 8 thiophene units and an extra diacetylene residue. The thiophene units closest to the acceptor moieties were substituted for EDOT moieties in both generations of dyes (identified by the suffix E) to aid with ICT. The synthesis of dyes **5T2A**, **5T2A-E**, **8T4A** and **8T4A-E** was accomplished as described in the ESI† and depicted in Scheme S1. The compound characterisation data are also provided in the ESI.†

### 2.2. Optical properties

The UV-vis absorption spectra of **5T2A**, **5T2A-E**, **8T4A** and **8T4A-E** are presented in Fig. 2 and were recorded as THF solutions ($1 \times 10^{-5}$ M). It is noteworthy that **5T2A-E** shows a bathochromic shift ($\lambda_{max}$ = 470 nm) in comparison with **5T2A** ($\lambda_{max}$ = 455 nm), and **8T4A-E** demonstrates similar behavior ($\lambda_{max}$ = 464 nm) in comparison with its counterpart **8T4A** ($\lambda_{max}$ = 446 nm, see Fig. 2). The π-extended dyes

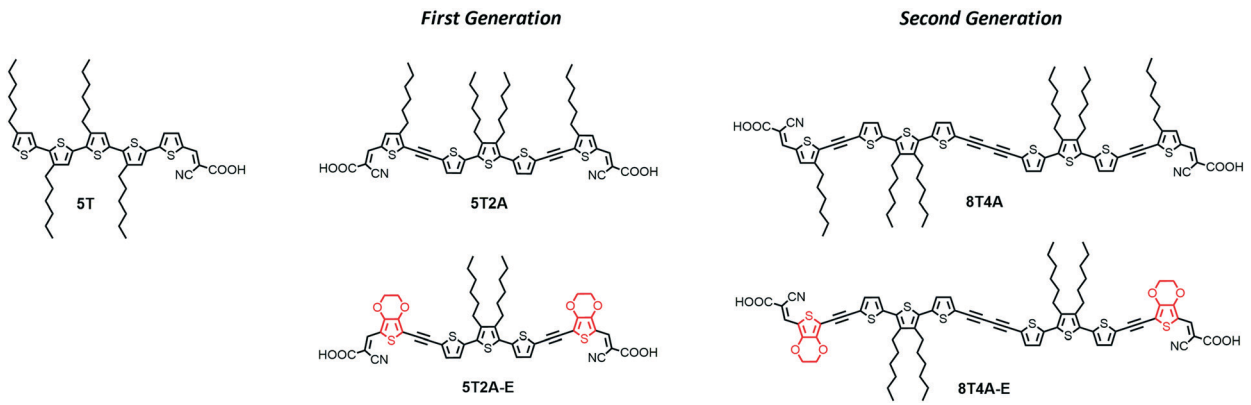


Fig. 1 Chemical structures of dye **5T** and the first- and second-generation dyes used in this study.

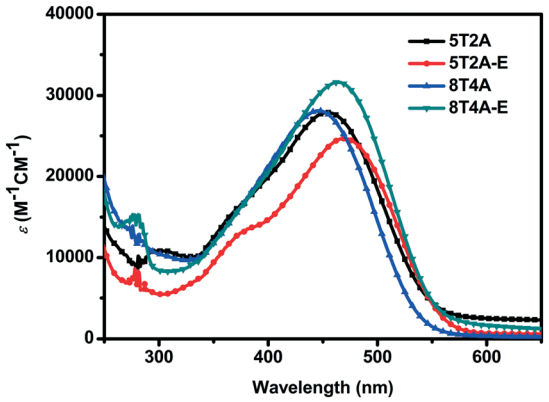


Fig. 2 Absorption spectra of **5T2A**, **5T2A-E**, **8T4A** and **8T4A-E** recorded in THF solution ($1 \times 10^{-5}$ M).

(featuring 8 thiophene units) showed slightly blue-shifted spectra in comparison with the 5 thiophene analogues. In addition, in comparison with the mono-anchoring dye **5T** that possesses an oligothiophene backbone featuring five thiophene units ($\lambda_{max}$ = 478 nm),[13,14] the second anchoring/acceptor moieties did not produce a red-shift of the $\lambda_{max}$. This can be attributed to the presence of the alkyne residues which, due to their electro-withdrawing nature, compromise ICT as they weaken the comparative electron accepting ability of the terminal acceptor.[35] The bands shown in the spectra are attributed to $S_0$–$S_1$ type transition due to the ICT between the electron rich units and the cyanoacrylate terminal acceptor moieties. All dyes present extinction coefficients within the same order of magnitude but with slight differences, ranging from 24 680 $M^{-1}$ $cm^{-1}$ (**5T2A-E**) to 31 630 $M^{-1}$ $cm^{-1}$ (**8T4A-E**). The optical gaps ($E_{opt}$) were estimated based on the onset values of absorption ($\lambda_{onset}$), and little difference was found with values ranging from *ca.* 2.09 eV (**5T2A-E**) to 2.14 eV (**5T2A**). All the optical and photophysical properties are presented in Table 1. In summary, the first- generation dyes displayed red-shifted spectra with a concomitant decrease in $E_{opt}$ with respect to their larger second-generation counterparts, while both generations showed slightly red-shifted $\lambda_{max}$ values for the dyes containing the **EDOT** units.

### 2.3. Electrochemical properties

To investigate the electrochemical properties of the dyes and determine the position of the energy levels relative to the conduction band of $TiO_2$ and the redox shuttles, square wave voltammetry measurements were performed in THF solution ($1 \times 10^{-3}$ M) *versus* the ferrocene/ferrocenium ($Fc/Fc^+$) redox couple. Evaluation of chemical/electrochemical reversibility was unfortunately not possible *via* cyclic voltammetry due to the low peak current intensity observed for this series (Fig. S10†). In the square wave voltammograms presented in Fig. 3, it is possible to observe one reduction ($E_{red}$) and one oxidation ($E_{ox}$) wave for each compound. Values of $E_{ox}$ and $E_{red}$ are presented in Table 1. The first-generation dyes show slightly more positive oxidation $E_{ox}$ (0.90 V for **5T2A** and 0.98 V for **5T2A-E**) than their second-generation counterparts (0.84 V for **8T4A** and 0.82 V for **8T4A-E**), with **5T2A-E** reaching the highest value of the series. All dyes display similar $E_{red}$ (*circa* −1.7 V) except for **5T2A**, which shows the least negative value (−1.34 eV). On the other hand, comparison of dyes with the same number of π-spacer units (**5T2A** and **5T2A-E**) shows a slightly positive shift in the $E_{ox}$ value for the **EDOT** containing **5T2A-E**. This minor difference in $E_{ox}$ is unexpected since **5T2A-E** should have a more electron-rich nature due to the **EDOT** unit, however, a similar result has been shown in the literature.[39] The $E_{ox}$ is an important parameter since it modulates the voltage loss in devices caused by excess driving force in the dye recovery process by redox mediators.[8,40] The electrochemical study shows that although these dyes have $E_{ox}$ positive enough to allow regeneration by the redox shuttle $I^-/I_3$, they are perhaps too positive and may induce recombination. The $E_{red}$ values are negative enough to ensure efficient electron injection into the conduction band of $TiO_2$.[12]

### 2.4. Computational studies

Density functional theory (DFT) calculations are applied in these molecular systems to gain more insight into their electronic properties. Firstly, theoretical studies were performed at the B3LYP/6-31G(d,p) level of theory in the gas phase to obtain a representation of molecular orbital distribution of **5T2A**, **5T2A-E**, **8T4A** and **8T4A-E**, which is provided in Fig. 4. All molecules display a linear optimised structure in the gas phase. The electron density plot of the highest occupied molecular orbital (HOMO) for **5T2A** and **5T2A-E** is localised over the whole molecule according to the calculations, whereas for **8T4A** and **8T4A-E** it is not found to extend to the acceptor groups and is mainly located on the oligothiophene residue. In the case of lowest unoccupied

Table 1 Summary of the optical and the electrochemical data of the di-anchoring dyes in this study

| Dye | $\lambda_{max}$ [a] [nm] | $\varepsilon_{max}$ [a] [$M^{-1}$ $cm^{-1}$] | $\lambda_{onset}$ [a] [nm] | $E_{opt}$ [b] [eV] | $E_{1/2ox}$ [c] [V] | $E_{1/2red}$ [c] [V] |
|---|---|---|---|---|---|---|
| **5T2A** | 455 | 27 890 | 578 | 2.14 | 0.90 | −1.34 |
| **5T2A-E** | 470 | 24 680 | 591 | 2.09 | 0.98 | −1.71 |
| **8T4A** | 446 | 28 120 | 565 | 2.19 | 0.84 | −1.76 |
| **8T4A-E** | 464 | 31 630 | 586 | 2.11 | 0.82 | −1.73 |

[a] Measured in tetrahydrofuran (THF, $1 \times 10^{-5}$ M). [b] Calculated using the formula $E_{opt} = 1240/\lambda_{onset}$. [c] Measured in THF ($1 \times 10^{-3}$ M) and calibrated *versus* the ferrocene/ferrocenium ($Fc/Fc^+$) redox couple.

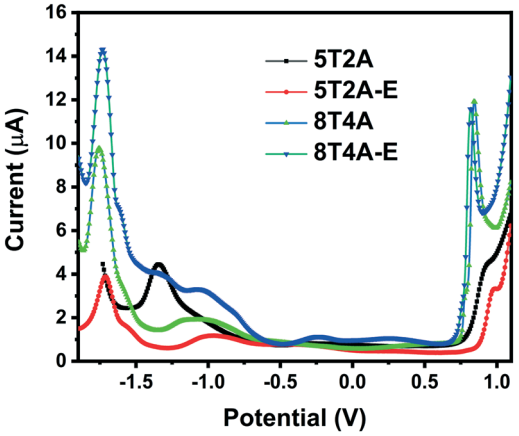


Fig. 3 Square wave voltammograms of **5T2A**, **5T2A-E**, **8T4A** and **8T4A-E**, recorded in THF ($1 \times 10^{-3}$ M), calibrated *versus* the ferrocene/ferrocenium ($Fc/Fc^{+}$) redox couple.

molecular orbital (LUMO), the electron density distribution is also localised over the whole molecule for **5T2A** and **5T2A-E**, resulting in a complete overlap between frontier orbitals. However, for **8T4A** and **8T4A-E**, the distribution is mostly localised towards the cyanoacrylate acceptor moieties not reaching the centre of the molecule, thus in these dyes the overlap between HOMO and LUMO happens to a lower extent than in the first-generation dyes.

To further understand the unimolecular properties and study the self-assembly tendencies of these dyes for a di-anchoring process, we used a computational method to estimate the number, distribution and properties of possible conformers of **5T2A**. The structural variation from **5T** to the first and second-generation dyes is expected to influence their structural conformation and self-assembly on the surface of the $TiO_2$ semiconductor. For instance, adjacent thiophenes usually adopt an *anti*-conformation due to non-covalent intramolecular CH–S interactions, and EDOT moieties usually cause a similar effect due to RO–S interactions.[33,34] Hence, oligothiophenes preferably adopt a linear arrangement that we consider non-ideal here for a di-anchoring process to happen, although evidences show that these rotational barriers can be overcome in a fluctuating environment at room temperature.[41,42] The acetylene residues in this work are thus expected to help to circumvent such conformational lock.[43–48]

The calculations were carried out using DFT at the ωB97X-D/6-31+G(d,p) level of theory, a method successfully applied in a similar study,[42] in the solvent state (in toluene and in THF at 300 K). A distribution analysis was performed to estimate the most likely distribution of conformer in solution. THF and toluene were chosen as their relative polarities are significantly different (polarity $\varepsilon$ values of 7.4257 and 2.3741 respectively) and therefore should show greater difference in the effect of solvent polarisation of the conformers. The diffuse and polarisation functions were used because it better accounts for the solvent effects.[49] Considering that **5T2A** has six points of rotation in total (omitting the hydroxy group of the carboxylic acid moiety), the number of possible conformers is $2^6$ (= 64) conformers (Fig. 5(a)). However due to symmetry a number of these conformers are energetically identical, therefore there are only 36 unique conformers (28 of them with a degeneracy of 2). Out of these conformers we identified 17 that adopt a linear shape, 14 that adopt a V shape and 5 that adopt a Z shape. Firstly, according to the calculations, the solvent polarity plays an important role in the distribution of accessible conformers at a given temperature. At 300 K, the most accessible conformer in toluene shows a Z-like shape (conformer 33), whereas in THF a linear (L) conformer (4) is the most favoured (see Fig. 5(b)). Furthermore, in THF, the relative population of other accessible conformers are considerably lower than in toluene. In toluene a total of five conformers were found at above 0.1 relative population

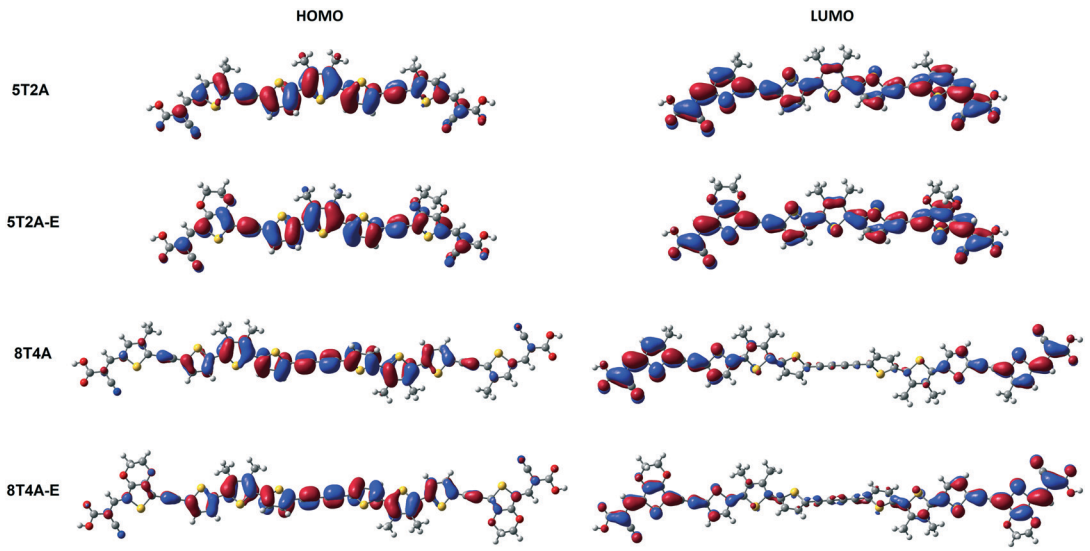


Fig. 4 Molecular orbital distribution of **5T2A**, **5T2A-E**, **8T4A** and **8T4A-E** computed at the B3LYP/6-31G(d,p) level.

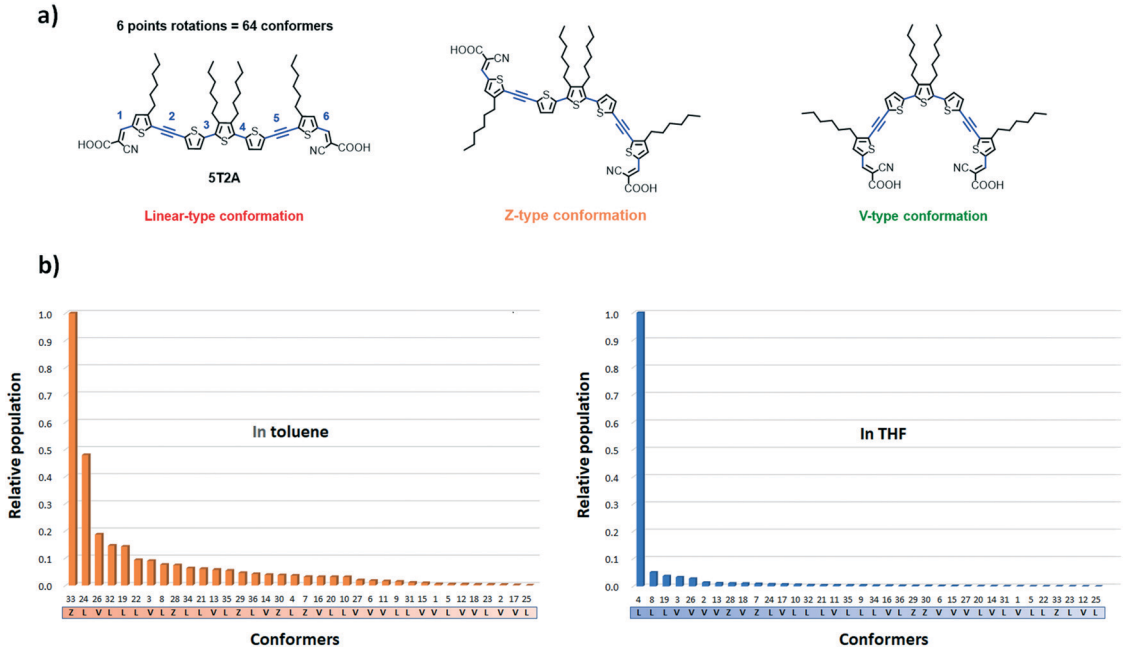


Fig. 5 (a) Schematic representation of **5T2A** in a linear (L), Z and V-type conformation. The points of rotations are represented in blue. (b) Relative population of independent conformers of **5T2A** in toluene (left) and in THF (right) at 300 K computed at the ωB97X-D/6-31+G(d,p) level of theory.

to conformer 33. The third most populated conformer (26) has a V-shape. In THF, the next most abundant conformer is predicted to have a population of 0.05 relative to 4.

The geometry of each conformer was optimised using the ωB97X-D/6-31+G(d,p) method (Table S3†). Importantly, in both solvents, the conformers are not significantly different in energy from one another. This suggests that the desirable V-shaped conformers are accessible at room temperature since the rotational cost is low.[41] Thus, the study shows that the V-shaped conformers are considerably lower in population, which could retard their uptake at the surface of $TiO_2$ *via* di-anchor and favour the mono-anchoring of dyes. The polarisation effect of the solvent suggests that toluene would favour a greater number of V-shaped conformers. Unfortunately, these dyes show considerably poorer solubility in toluene than in THF which can limit their study in the device.

### 2.5. Device performance

The four dyes, **5T2A**, **5T2A-E**, **8T4A** and **8T4A-E**, were tested in dye-sensitized solar cells (DSSCs) with the structure Fluorine-doped $SnO_2$ (FTO)/compact $TiO_2$/mesoporous $TiO_2$/dye/$I^-/I_3^-$ electrolyte/Pt/FTO. **5 T** dye was used as a reference. The current density–voltage (J–V) curves of the champion cells are shown in Fig. 6, with the values summarised in Table 2. The statistics are shown in Fig. S11.† All dyes in the series exhibited a PCE of around 2–3%, compared to the reference **5T** dye at around 5–6%. The maximum PCEs achieved for the best cells were 3.70% with **5T2A** or **5T2A-E**, and 2.82% with **8T4A** or **8T4A-E**. Overall, all A–$\pi_n$–A dyes showed lower performance in respect to the $\pi_n$–A **5T** dye. The relatively low $V_{OC}$ range (*circa* 0.5–0.6 V) suggests that recombination is facilitated in these systems. One possible cause for this is the highly positive $E_{ox}$ of the new dyes, which could act as a driving force for the $TiO_2$ conduction band electrons to recombine with the oxidised dye. Within the series, the first-generation dyes, **5T2A** and **5T2A-E**, achieved higher PCE compared to the second generation, mainly attributed to larger current generation. Larger current can often arise from higher extinction coefficient of the dyes, however in our case this appears to be irrelevant. It is therefore likely that the molecular size or/and anchoring of the dyes is contributing to the performance trends.

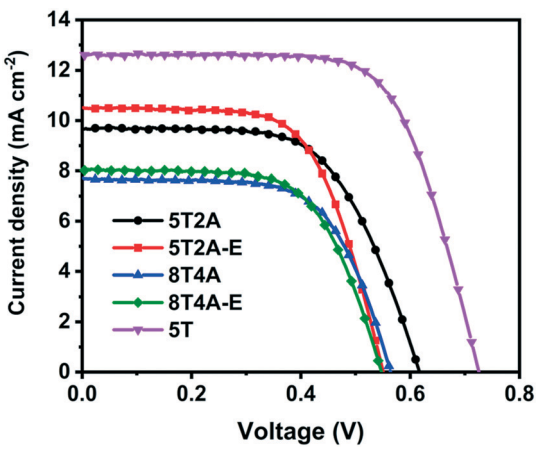


Fig. 6 J–V curves of the best DSSCs employing **5T2A**, **5T2A-E**, **8T4A** and **8T4A-E** as light absorbers, with **5T** dye as a reference.

Table 2 Summary of photovoltaic characteristics of the DSSCs employing **5T2A**, **5T2A-E**, **8T4A** and **8T4A-E** as light absorbers with $I^-/I_3^-$ as electrolyte. **5 T** was used as the reference dye. The mean and standard deviation of 5 cells are described in brackets

| Dye | $J_{SC}$ (mA cm$^{-2}$) | $V_{OC}$ (V) | ff | PCE (%) |
|---|---|---|---|---|
| **5T2A** | 9.68 (8.8 ± 1.3) | 0.62 (0.60 ± 0.07) | 0.62 (0.64 ± 0.06) | 3.70 (3.4 ± 0.3) |
| **5T2A-E** | 10.5 (9.3 ± 1.3) | 0.55 (0.53 ± 0.03) | 0.64 (0.62 ± 0.02) | 3.70 (2.8 ± 0.7) |
| **8T4A** | 7.69 (6.8 ± 1.4) | 0.56 (0.54 ± 0.02) | 0.65 (0.62 ± 0.06) | 2.82 (2.4 ± 0.5) |
| **8T4A-E** | 8.03 (8.0 ± 0.7) | 0.55 (0.51 ± 0.02) | 0.64 (0.59 ± 0.06) | 2.82 (2.4 ± 0.4) |
| **5T** | 12.6 (12.1 ± 0.6) | 0.72 (0.70 ± 0.03) | 0.69 (0.66 ± 0.03) | 6.24 (5.6 ± 0.4) |

Computational studies suggest that the dyes in the series occupy *circa* 4 nm$^2$ when mono-anchored and 9 nm$^2$ when di-anchored to the $TiO_2$. These values will lead to estimated dye amounts of 6.64 $10^{-8}$ mol cm$^{-2}$ for mono-anchoring and 2.95 $10^{-8}$ mol cm$^{-2}$ for di-anchoring. Dye uptake for **5T2A**, **5T2A-E**, **8T4A** and **8T4A-E** was measured from UV-vis absorption and derived as 9.60 $10^{-8}$ mol cm$^{-2}$, 8.38 $10^{-8}$ mol cm$^{-2}$, 6.01 $10^{-8}$ mol cm$^{-2}$ and 2.68 $10^{-8}$ mol cm$^{-2}$, respectively. Comparing these values with the estimated amount in each case indicate that **5T2A**, **5T2A-E** and **8T4A** are mono-anchored, while **8T4A-E** may or may not be di-anchored. This follows the suggestion from the computational studies, where the A–$\pi_n$–A dyes prefer linear binding to the $TiO_2$ over di-anchoring. In the case of mono-anchoring of the A–$\pi_n$–A dye, the electron pathway within the dye is deviated into two opposite directions, with one end receding from the $TiO_2$ network. The remote acceptor residue would then work as an unwanted electron sink and recombination site, leading to lower current and voltage. However, as indicated above, di-anchoring may occur for **8T4A-E**, due to the rapidly fluctuating conformation of the dye molecules at the liquid/solid interface during dye loading. However, the poor current and voltage trends displayed by the larger **8T4A** and **8T4A-E** dyes suggest that the larger structures lead to low dye uptake and recombination at the $TiO_2$/electrolyte interface, due to the creation of large voids when di-anchored.

Poor solubility of the dyes is also detrimental to attaining higher performance. The incident photon-to-current efficiency (IPCE) data of DSSCs employing the most efficient A–$\pi_n$–A dye, **5T2A** (Fig. S12†), indicates that the use of THF leads to lower IPCE, hence lower current. However, in our case, the low solubility of the four dyes, especially **8T4A** and **8T4A-E** in most organic solvents left us with the sole choice to employ a THF-based binary dye bath system for sufficient dye uptake. This could also be one of the causes of their low performance. Dye bath solvent effects have been studied by Tian *et al.*,[50] where our findings are relatively consistent with their suggestions.

The EDOT-substituted **5T2A-E** and **8T4A-E** displayed slightly higher current compared to their counterparts, which is expected due to the improved electron donating ability by incorporation of the EDOT residues. It is interesting to note that the dye uptake is lower for these dyes. On the other hand, the $V_{OC}$ appeared to decrease slightly, resulting in a lower average PCE in the case of **5T2A-E** and similar in the case of **8T4A-E**.

## 3. Conclusions

The oligothiophene based dyes composed of 5 and 8 thiophenes and possessing di-anchoring architecture were synthesized and compared with **5T** in terms of photophysical and DSSC properties. Within this series, slightly red-shifted spectra were observed for the dyes containing **EDOT** residues, whereas the larger second-generation dyes showed slightly blue shifted spectra in comparison with their 5-thiophene analogues. The blue-shifted spectra of this series with respect to **5T** were attributed to the presence of acetylene residues. By comparing the first-generation (**5T2A** and **5T2A-E**) and second-generation (**8T4A** and **8T4A-E**) systems, the former shows better performance in general. The trend is irrelevant to the absorption properties and is likely to come from the dye architecture and solubility.

The computational studies implied that although the V- and U-shaped conformers are perfectly accessible at room temperature, this series likely show a considerable population of mono-anchored dyes at the surface of the $TiO_2$ adopting a more linear conformation. However, as demonstrated for **5T2A**, solvents with higher polarity may have a detrimental effect in allowing molecular motion by stabilising linear conformations. This is problematic due to the low solubility of the dyes in less polar solvents. The dye uptake analysis suggests that **5T2A**, **5T2A-E** and **8T4A** have mono-anchored, while **8T4A-E** is possibly di-anchored. Mono-anchored A–$\pi_n$–A dyes are detrimental to the extraction of charge and $J_{sc}$, since the remote acceptor residue works as an electron sink and recombination site.

Within the series, **5T2A** exhibits the highest current density, voltage and PCE, presumably due to the higher dye uptake and higher solubility. The optical/electrochemical properties of this series have been demonstrated to be favourable as a DSSC dye sensitizer, however the overall photovoltaic performance does not appear to be advantageous over the reference $\pi_n$–A **5T dye**. Future designing of such dyes should involve further consideration on compactness, rigidity, and solubility. Overall, 'donor-free' oligothiophene based A–$\pi_n$–A dyes were introduced for the first time, and their ability as DSSC sensitizers were demonstrated. We believe that our

 

study will serve as pathways towards improved designing of such dye families.

# 4. Experimental

### 4.1. Synthesis

Reagents were purchased from Sigma Aldrich®, Fluorochem®, TCI®, Alfa Aesar®, Acros® or Fisher Scientific® and used as received. Dry solvents were obtained either from Innovative Technology inc. Pure Solv 400-5-MD solvent purification system (activated alumina columns) or Sigma Aldrich®. Column chromatography was carried out using silica gel (Sigma-Aldrich) 40–63 nm particle size, 60 Å pore size. The solvent system is specified in each experiment. Thin-layer chromatography (TLC) was performed using Merck silica gel 60 covered aluminium plates F254. NMR spectra were obtained with either a Bruker Avance III 400 or a Bruker Avance III 500 spectrometers. Mass spectra were obtained from the mass spectrometry service at the University of Glasgow and from the EPSRC UK National Mass Spectrometry Facility at Swansea University. All the spectroscopic (except NMR) and electrochemical data were processed using Origin Pro 8.5 software suite.

### 4.2. Optical and electrochemical properties

UV-vis spectra were recorded on a Perkin Elmer 25 UV/VIS Spectrometer at room temperature. Voltammograms were recorded on a CH Instrument Electrochemical Workstation (CHI 440a), Austin, TX, USA. Solutions were prepared in THF ($1 \times 10^{-3}$ M) containing TBA.$PF_6$ (0.1 M) as electrolyte. The scan rate of 0.07 V $s^{-1}$ was utilized. The redox couples are reported *versus* the ferrocene/ferrocenium ($Fc/Fc^+$) redox couple, using a 1.6 mm diameter platinum working electrode, a platinum wire counter electrode and a silver wire pseudo reference electrode.

### 4.3. Computational studies

Density functional theory (DFT) calculations were performed using Gaussian 09 software suite.[51] In the gas phase, molecular geometries were initially optimised semi-empirically (PM6) and then re-optimised by DFT (B3LYP/6-31G(d,p)). In the conformational studies ωB97X-D/6-31+G(d, p) (solution state) was used. Some conformers were found to have negative frequency which were identified as transition states between two more stable conformers in energy. To facilitate the convergence of the geometry optimisations, the hexyl chains were replaced by methyl groups.

### 4.4. Solar cell fabrication

Fluorine-doped tin oxide (FTO) glass (TCO22-7/Li, Solaronix) substrates were cleaned by sonication in 2% Decon 90 (Decon Laboratories) aq., deionized water, acetone and ethanol for 15 min each, followed by UV/$O_3$ treatment for 20 min to make the surface hydrophilic. The blocking $TiO_2$ layer was formed by immersing the substrates in 40 mM $TiCl_4$ aq. at 80 °C for 30 min and rinsing with water. The mesoporous $TiO_2$ layer was formed by screen-printing Dyesol 18NR-D (transparent layer, thickness 4 μm) and 18NR-AO (scattering layer, 4 μm) paste. The photoanodes were gradually heated to 500 °C and annealed for 15 min in a programmable furnace. Upon cooling, a second $TiCl_4$ treatment was applied and the films were annealed at 500 °C for 30 min. Dye loading was initiated while the films were warm (>80 °C) and was performed overnight. **5T** dye was used as a reference. The solvent system and concentration were optimised for each dye (full details in Table S4†). The cathodes were fabricated by doctor-blading Platisol T/SP (Solaronix) on cleaned FTO substrates and annealing at 400 °C for 15 min to obtain a Pt-coated FTO glass. The anode and cathode were assembled using a 25 μm Surlyn film (Du Pont) as spacer. The $I^-/I_3^-$-electrolyte was injected under vacuum through a pre-drilled hole in the cathode. The composition of the electrolyte used in the study was 0.1 M LiI, 0.05 M $I_2$, 0.6 M 1,2-dimethyl-3-propylimidazolium iodide (DMPII) and 0.5 M 4-*tert*-butylpyridine in acetonitrile. The hole was finally sealed with a piece of Surlyn and cover glass slip.

### 4.5. Solar cell characterization

The current–voltage (*J–V*) curves were recorded on an Autolab PGSTAT30 potentiostat. The cells were irradiated with an AM 1.5G simulated sunlight at 100 mW $cm^{-2}$, generated by a Sciencetech SLB-300A compact solar simulator class AAA. The light intensity was calibrated by a Si reference cell before each measurement. A black mask with an aperture size of 0.2827 $cm^2$ was used to define the active area.

The incident photon-to-current conversion efficiency (IPCE) curves were recorded on a Bentham PVE300 EQE/IQE system in DC mode. The incident light was calibrated with a reference silicon photodiode within the range of 300–1000 nm.

The dyes were desorbed from the $TiO_2$ by immersion in 0.1 M tetrabutylammonium hydroxide ethanol/methanol 9 : 1 (v/v) solution. Dye uptake was derived from the UV/Vis absorption peak of the resulting solutions.

# Conflicts of interest

There are no conflicts to declare.

# Acknowledgements

JMS acknowledges the *Coordenação de Aperfeiçoamento de Pessoal de Nível Superior - Brasil (CAPES) - Finance Code 001* for PhD funding. JMS thanks EPSRC UK National Mass Spectrometry Facility at Swansea University. ET thanks the Japan Student Services Organization (JASSO) for a PhD studentship. GC acknowledges the EPSRC for funding (EP/E036244/1). Open data available at: http://dx.doi.org/10.5525/gla.researchdata.1128. We acknowledge the Centre for Plastic Electronics (CPE), Imperial College London for access to their IPCE facility.

## Notes and references

1 A. Yella, C. Mai, S. M. Zakeeruddin, S. Chang, C. Hsieh, Y. Yeh and M. Grätzel, *Angew. Chem.*, 2014, **126**, 3017–3021.
2 N. Manfredi, B. Cecconi and A. Abbotto, *Eur. J. Org. Chem.*, 2014, 7069–7086.
3 B. O'Regan and M. Grätzel, *Nature*, 1991, **353**, 737–740.
4 A. Hagfeldt, G. Boschloo, L. Sun, L. Kloo and H. Pettersson, *Chem. Rev.*, 2010, **110**, 6595–6663.
5 S. Mathew, A. Yella, P. Gao, R. Humphry-baker, B. F. E. Curchod, N. Ashari-astani, I. Tavernelli, U. Rothlisberger, K. Nazeeruddin and M. Gra, *Nat. Chem.*, 2014, **6**, 242–247.
6 J. Gong, K. Sumathy, Q. Qiao and Z. Zhou, *Renewable Sustainable Energy Rev.*, 2017, **68**, 234–246.
7 P. P. Kumavat, P. Sonar and D. S. Dalal, *Renewable Sustainable Energy Rev.*, 2017, **78**, 1262–1287.
8 W. Zhang, Y. Wu, H. W. Bahng, Y. Cao, C. Yi, Y. Saygili, J. Luo, Y. Liu, L. Kavan, J. Moser, A. Hagfeldt, H. Tian, S. M. Zakeeruddin, W. Zhu and M. Gr, *Energy Environ. Sci.*, 2018, **10**, 8–10.
9 X. Zhang, A. Bolag, W. Yun, C. Eerdun, Y. Du, J. Ning and H. Alata, *Chem. Lett.*, 2018, **48**, 204–207.
10 P. Kumaresan, S. Vegiraju, Y. Ezhumalai, S. L. Yau, C. Kim, W. H. Lee and M. C. Chen, *Polymer*, 2014, **6**, 2645–2669.
11 X. Dai, H. Feng, W. Chen, Y. Yang, L. Nie, L. Wang, D. Kuang, H. Meier and D. Cao, *Dyes Pigm.*, 2015, **122**, 13–21.
12 H. L. Jia, M. D. Zhang, W. Yan, X. H. Ju and H. G. Zheng, *J. Mater. Chem. A*, 2016, **4**, 11782–11788.
13 Y. Hu, A. Ivaturi, M. Planells, C. L. Boldrini, A. O. Biroli and N. Robertson, *J. Mater. Chem. A*, 2016, **4**, 2509–2516.
14 A. Abate, M. Planells, D. J. Hollman, S. D. Stranks, A. Petrozza, A. R. S. Kandada, Y. Vaynzof, S. K. Pathak, N. Robertson and H. J. Snaith, *Adv. Energy Mater.*, 2014, **4**, 1–7.
15 A. Listorti, B. O'Regan and J. R. Durrant, *Chem. Mater.*, 2011, **23**, 3381–3399.
16 N. T. Hai, L. Q. Bao, S. Thogiti, R. Cheruku, K. S. Ahn and J. H. Kim, *J. Nanosci. Nanotechnol.*, 2017, **17**, 3181–3187.
17 W. C. Chen, S. Nachimuthu and J. C. Jiang, *Sci. Rep.*, 2017, **7**, 1–13.
18 I. Arbouch, D. Cornil, Y. Karzazi, B. Hammouti, R. Lazzaroni and J. Cornil, *Phys. Chem. Chem. Phys.*, 2017, **19**, 29389–29401.
19 L. Zhang and J. M. Cole, *ACS Appl. Mater. Interfaces*, 2015, **7**, 3427–3455.
20 R. Kesavan, F. Attia, R. Su, P. Anees, A. El-Shafei and A. V. Adhikari, *J. Phys. Chem. C*, 2019, **123**, 24383–24395.
21 Ö. Birel, S. Nadeem and H. Duman, *J. Fluoresc.*, 2017, **27**, 1075–1085.
22 S. S. M. Fernandes, M. C. R. Castro, A. I. Pereira, A. Mendes, C. Serpa, J. Pina, L. L. G. Justino, H. D. Burrows and M. M. M. Raposo, *ACS Omega*, 2017, **2**, 9268–9279.
23 G. Koyyada, R. K. Chitumalla, S. Thogiti, J. H. Kim, J. Jang, M. Chandrasekharam and J. H. Jung, *Molecules*, 2019, **24**, 1–18.
24 P. Naik, R. Su, M. R. Elmorsy, A. El-Shafei and A. V. Adhikari, *Photochem. Photobiol. Sci.*, 2018, **17**, 302–314.
25 C. Qin, A. Mirloup, N. Leclerc, A. Islam and A. El-shafei, *Adv. Energy Mater.*, 2014, **2**, 2–7.
26 Y. C. Chen and J. T. Lin, *Sustainable Energy Fuels*, 2017, **1**, 969–985.
27 H. Klfout, A. Stewart, M. Elkhalifa and H. He, *ACS Appl. Mater. Interfaces*, 2017, **9**, 39873–39889.
28 G. Wu, F. Kong, Y. Zhang, X. Zhang, J. Li, W. Chen, W. Liu, Y. Ding, C. Zhang, B. Zhang, J. Yao and S. Dai, *J. Phys. Chem.*, 2014, **118**, 8756–8765.
29 Y. S. Yang, H. Do Kim, J. H. Ryu, K. K. Kim, S. S. Park, K. S. Ahn and J. H. Kim, *Synth. Met.*, 2011, **161**, 850–855.
30 Y. H. Lee, H. J. Yun, S. K. Choi, Y. S. Yang, T. Park, K. S. Ahn, T. Suresh and J. H. Kim, *Synth. Met.*, 2016, **217**, 248–255.
31 H. Wu, Z. Huang, T. Hua, C. Liao, H. Meier, H. Tang, L. Wang and D. Cao, *Dyes Pigm.*, 2019, **165**, 103–111.
32 U. Eiamprasert, J. Sudchanham and P. Surawatanawong, *J. Photochem. Photobiol., A*, 2018, **352**, 86–97.
33 Y.-J. Cheng, S.-H. Yang and C.-S. Hsu, *Chem. Rev.*, 2009, **109**, 5868–5923.
34 Y. Wang, Q. Liao, G. Wang, H. Guo, X. Zhang, M. A. Uddin and X. Guo, *Chem. Mater.*, 2017, **29**, 4109–4121.
35 C. Teng, X. Yang, C. Yang, H. Tian, S. Li, X. Wang, A. Hagfeldt and L. Sun, *J. Phys. Chem. C*, 2010, **114**, 11305–11313.
36 H. Jia, K. Shen, X. Ju, M. Zhang and H. Zheng, *New J. Chem.*, 2016, **40**, 2799–2805.
37 A. F. Buene, E. E. Ose, A. G. Zakariassen, A. Hagfeldt and B. H. Hoff, *J. Mater. Chem. A*, 2019, **7**, 7581–7590.
38 R. Tarsang, V. Promarak, T. Sudyoadsuk, S. Namuangruk, N. Kungwan, P. Khongpracha and S. Jungsuttiwong, *RSC Adv.*, 2015, **5**, 38130–38140.
39 Z. Shen, X. Zhang, F. Giordano, Y. Hu and J. Hua, *Mater. Chem. Front.*, 2016, **1**, 181–189.
40 A. Baheti, P. Singh, C. P. Lee, K. R. J. Thomas and K. C. Ho, *J. Org. Chem.*, 2011, **76**, 4910–4920.
41 N. E. Jackson, B. M. Savoie, K. L. Kohlstedt, M. Olvera De La Cruz, G. C. Schatz, L. X. Chen and M. A. Ratner, *J. Am. Chem. Soc.*, 2013, **135**, 10475–10483.
42 C. Mcdowell, K. Narayanaswamy, B. Yadagiri, M. C. Heifner, V. Gupta, C. Risko and P. Singh, *J. Mater. Chem. A*, 2018, **6**, 383–394.
43 K. Nakao, M. Nishimura, T. Tamachi, Y. Kuwatani, H. Miyasaka, T. Nishinaga and M. Iyoda, *J. Am. Chem. Soc.*, 2006, **128**, 16740–16747.
44 D. K. Frantz, A. Linden, K. K. Baldridge and J. S. Siegel, *J. Am. Chem. Soc.*, 2012, **134**, 1528–1535.
45 M. El Garah, A. Dianat, A. Cadeddu, R. Gutierrez, M. Cecchini, T. R. Cook, A. Ciesielski, P. J. Stang, G. Cuniberti and P. Samorì, *Small*, 2016, **12**, 343–350.
46 M. D. Peeks, P. Neuhaus and H. L. Anderson, *Phys. Chem. Chem. Phys.*, 2016, **18**, 5264–5274.
47 S. Q. Zhang, Z. Y. Liu, W. F. Fu, F. Liu, C. M. Wang, C. Q. Sheng, Y. F. Wang, K. Deng, Q. D. Zeng, L. J. Shu, J. H. Wan, H. Z. Chen and T. P. Russell, *ACS Nano*, 2017, **11**, 11701–11713.

48 I. Gru, H. J. Eggimann, L. M. Herz and H. L. Anderson, *J. Am. Chem. Soc.*, 2019, **141**, 7965–7971.

49 D. J. Carmona, D. R. Contreras, O. A. Douglas-Gallardo, S. Vogt-Geisse, P. Jaque and E. Vöhringer-Martinez, *Theor. Chem. Acc.*, 2018, **137**, 1–11.

50 H. Tian, X. Yang, R. Chen, R. Zhang, A. Hagfeldt and L. Sun, *J. Phys. Chem. C*, 2008, **112**, 11023–11033.

51 M. J. Frisch, G. W. Trucks, H. B. Schlegel, G. E. Scuseria, M. A. Robb, J. R. Cheeseman, G. Scalmani, V. Barone, B. Mennucci, G. A. Petersson, H. Nakatsuji, M. Caricato, X. Li, H. P. Hratchian, A. F. Izmaylov, J. Bloino, G. Zheng, J. L. Sonnenberg, M. Hada, M. Ehara, K. Toyota, R. Fukuda, J. Hasegawa, M. Ishida, T. Nakajima, Y. Honda, O. Kitao, H. Nakai, T. Vreven, J. A. J. Montgomery, J. E. Peralta, F. Ogliaro, M. Bearpark, J. J. Heyd, E. Brothers, K. N. Kudin, V. N. Staroverov, R. Kobayashi, J. Normand, K. Raghavachari, A. Rendell, J. C. Burant, S. S. Iyengar, J. Tomasi, M. Cossi, N. Rega, J. M. Millam, M. Klene, J. E. Knox, J. B. Cross, V. Bakken, C. Adamo, J. Jaramillo, R. Gomperts, R. E. Stratmann, O. Yazyev, A. J. Austin, R. Cammi, C. Pomelli, J. W. Ochterski, R. L. Martin, K. Morokuma, V. G. Zakrzewski, G. A. Voth, P. Salvador, J. J. Dannenberg, S. Dapprich, A. D. Daniels, Ö. Farkas, J. B. Foresman, J. V. Ortiz, J. Cioslowski and D. J. Fox, *Gaussian 09, Revision D.01*, 2009.